Chapter – II

Materials and Experimental Techniques

Abstract

A brief review of the concept of polymer composites and general descriptions of the experimental methods and tools are given in this chapter. The working principles and operation of Pelletron accelerators has been conversed. Different characterization techniques have been used to do off-line analysis of the pristine and irradiated samples in this work. These techniques with their proper specifications and operating principle have been described.

2.0 Introduction

This chapter deals with the detailed description of the material (polymers and fillers) used for the present study, the working principle of Pelletron and different techniques used for the offline measurement of pristine and irradiated samples. Detail explanation of following is considered in this chapter.

- Materials: Properties and preparation methods of Polymer/fillers
- Working principle and details of Pelletron
- Sample preparation and thickness measurement
- Calculation of ion range and its energy loss by SRIM code
- X-ray diffraction
- UV-visible analysis
- Differential Scanning Calorimetry (DSC)
- Scanning electron microscopy (SEM)
- Superconducting Quantum Interference Device (SQUID)
- AC electric response

2.1 Materials

2.1.1 Selected polymers:

(a) Polymethyl methacrylate (PMMA)

PMMA (polymethyl methacrylate) is a versatile polymeric material that is well suited for many imaging and non-imaging microelectronic applications. PMMA is most commonly used as a high resolution positive resist for direct write e-beam as well as x-ray and deep UV micro lithographic processes. PMMA is also used as a protective coating for wafer thinning, as a bonding adhesive and as a sacrificial layer [1, 2].

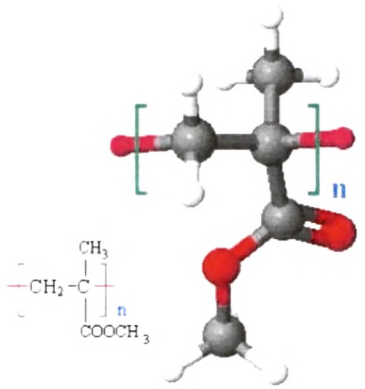

IUPAC name: Poly (methyl 2-methylpropenoate)

Molecular formula: $(C_5O_2H_8)_n$

PMMA is an amorphous, linear polymer valued for its hardness, rigidity, transparency and weathering resistance. But modified PMMA was even more outstanding performance edge. They are widely used in optical instruments, construction areas, can be used as medical devices, such as additional limbs, dentures, medical optical basic raw material. It is still used as a glass substitute for aerospace equipment, light cover, surface cover plates, car and motorcycle windshields [3,4].

(b) Polystyrene (PS)

Polystyrene is a "polymer of styrene." Polymers are large molecules consisting of adjoined identical molecules, and styrene is a colorless, oily liquid. When polystyrene is made, its structure is that of a rigid transparent thermoplastic. It is one of the most

common types of plastic, and it can be found in the home, in the office, at industrial sites, and just about any other place you would find plastics. Businesses rely on polystyrene for a number of uses, including manufacturing, packaging, and construction.

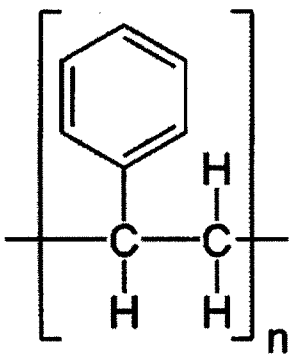

IUPAC name: Poly(1-phenylethane-1,2-diyl)

Molecular formula: $(C_8H_8)_n$

Polystyrene is a hard, crystal clear, amorphous solid at room temperature that exhibits high stiffness, good dimensional stability, moderately high heat deflection temperature and excellent electrical insulating properties. It retains its stiffness to about 20-25°C below glass transition temperature (Tg). However, polystyrene will become softer as it getting closer to its Tg. Above Tg, polystyrene behaves under stress as a viscous fluid. When the temperature is further raised, it will become rubbery and highly extensible. Polystyrene is a very important one due to its easy processibility, low density, low price, good optical transparency, and acceptable thermal insulation and damping properties. However, it is brittle under impact and the resistance towards surfactants and solvent is very poor [5, 6].

2.1.2 Fillers:

(a) Silver nanoparticles (Ag)

Appearance: Grey

Silver nanoparticles have unique optical, electrical, and thermal properties and are being incorporated into products that range from photovoltaics to biological and chemical sensors. Examples include conductive inks, pastes and fillers which utilize silver nanoparticles for their high electrical conductivity, stability, and low sintering temperatures [7]. Additional applications include molecular diagnostics and photonic devices, which take advantage of the novel optical properties of these nanomaterials. An increasingly common application is the use of silver nanoparticles for antimicrobial coatings, and many textiles, keyboards, wound dressings, and biomedical devices [8].

(b) Nickel nanoparticles (Ni)

Appearance: Black

As an important transition metal, Ni nanoparticles have wide ranging applications in the fields of permanent magnets, magnetic fluids, magnetic recording media, solar energy absorption, fuel cell electrodes, catalysts etc. So the synthesis of Ni nanoparticles has attracted considerable attention. The magnetic fluid made of nickel nanoparticles provides excellent properties. It is widely used for sealants, shock absorption materials, medical equipment, and optical displays. Due to its large surface and high activity, nickel nanoparticles are efficient catalysts for chemical reactions such as hydrogenation and treatment of exhaust to reduce harmful chemicals. Conductive paste is commonly used for wiring and packaging. In the microelectronics industry, it plays an important role in the miniturization of electronic devices and

circuits. They can be made into electrodes with a large surface area to considerably improve energy density [9-12].

(c) Copper nanoparticles (Cu)

Appearance: Dark red (brown)

Copper is an essential trace element in animals and plants, but in excess copper is toxic. Due to its high electrical conductivity, large amounts of copper are used by the electrical industry for wire. Recent research reveals that diluted magnetic semiconductors can be produced using Copper. Copper is also resistant to corrosion caused by moisture, making it a widely used material in pipes, coins, and jewellery. The key applications of copper nanoparticles are listed here: Acts as an anti-biotic, anti-microbial, and anti-fungal agent when added to plastics, coatings, and textiles, Copper diet supplements with efficient delivery characteristics, High strength metals and alloys, EMI shielding, Heat sinks and highly thermal conductive materials, Efficient catalyst for chemical reactions and for the synthesis of methanol and glycol, electronics, displays, and transmissive conductive thin film applications. Copper nanoparticles application research is ongoing to discover their potential dielectric, magnetic, electrical, optical, imaging, catalytic, biomedical and bioscience properties [13, 14].

2.1.3 Polymer nanocomposites:

Polymer composites were prepared by doping different concentrations i.e. 5, 10, 15 wt. % of silver, nickel, copper nanoparticles in PMMA and PS with THF (Tetra hydro furan) and toluene as a solvent. The mixture of filler and polymers was stirred for 2-3

hours and sonicate for few minutes to get dispersion in matrix and then pour into petri dishes. Thus the composite films were prepared by casting method.

2.1.4. Thickness measurement of the composite films:

The thickness of as synthesized composites was measured by a sensitive digital instrument. Sensitivity of the instrument was 0.001mm. The thickness of polymers was measured at 8-10 places randomly chosen and average of it was taken. The calculated thickness was listed in Table 2.1.

Table 2.1 Thickness of the polymers

Sample	Thickness
Pure PMMA films	110 μm
PMMA + Ag	110 μm
PMMA + Ni	120 μm
PMMA + Cu	120 μm
Pure PS films	110 μm
PS + Ag	120 μm
PS + Ni	120 μm
PS + Cu	110 μm

2.2 Ion beam irradiation

Energetic ions for polymer irradiation can be produced in several ways. Nowadays the common approach is the use of ion implanters and ion accelerators. The basic difference between both is, the available energy range and the ion beam currents delivered from both the machines. Ion implanters usually work in the range of 10 to several 100 keV energy interval delivering high currents that can go from tens of μA to few tens of mA. Ion accelerators work in the MeV energy region but with lower currents. The present work delivers the high energetic particle accelerator.

2.2.1 The Pelletron accelerator:

A high energy Pelletron accelerator, tandem Van de Graaff type accelerator, for basic and applied research in nuclear physics, atomic physics, materials science, biosciences and other allied fields is running at IUAC. This Linear accelerator is planned as a booster accelerator. A 15UD Pelletron accelerator is capable of delivering any ion from proton to uranium up to energy of a few hundred MeV depending upon the nature of ion. It has been installed at IUAC, New Delhi by the Electrostatic International Inc., USA. This is a tandem Van de Graaff accelerator, in which the charge carrier belt is replaced by a chain of pellets. The digit 15 stands for 15 MV terminal voltage and UD stands for Unit Double. The whole machine is mounted vertically; a schematic of the machine is shown in Fig 2.1.

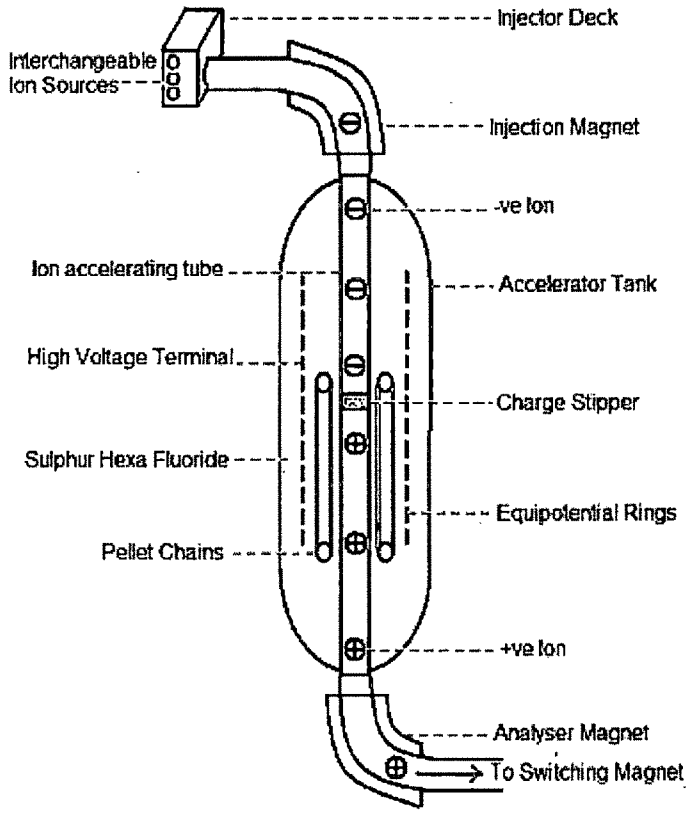

Fig. 2.1 Schematic of Pelletron accelerator

The Pelletron accelerator has an insulating steel tank of height 26.57 and width 5.5 m. In order to attain insulation (to prevent sparking/discharging) the tank is filled with sulfur hexafluoride (SF6) gas at a pressure of 4.0 Torr. The SNICS (Source of Negative Ion by Cesium Sputtering) ion source acts as a source of negative ions that are momentum analyzed by the injector magnets. A high voltage terminal with 1.52 mm diameter and 3.81 mm length at the middle of the tank can be charged by a high potential varied from 4 to 15 MV using an electrostatic charge transfer device. This terminal is connected to the tank vertically through ceramic titanium tubes known as the accelerating tubes. A potential gradient is maintained with the help of these tubes.

Negative ions from the ion source are injected towards the terminal and are stripped off a few electrons through stripper foils. The yield is converted into positive ions.

These ions are further accelerated as they proceed to the bottom of the tank at ground potential. As a result the ions from the accelerator gain energy, given by Eq. (1.1) as,

$$E = V_{\pi} (q + 1) \text{ MeV} \qquad (2.1.1)$$

where V_{π} is terminal potential and q is the number of positive charges (charge states) on the ions after stripping.

Thus a heavy ion of charge state q will attain a final kinetic energy equal to $(q + 1) \times 15$ MeV. Thus protons accelerated to a full terminal voltage would have energy of 30 MeV. By using appropriate magnets with respect to the charge states and energies, the high energetic ions are analyzed and are bent at 90° with respect to vertical position by using analyzer magnet. These redirected ions are directed to the desired experimental area in the beam hall with the help of multi-port switching magnet. Fig. 2.2 shows that the materials science chamber for ion beam irradiation.

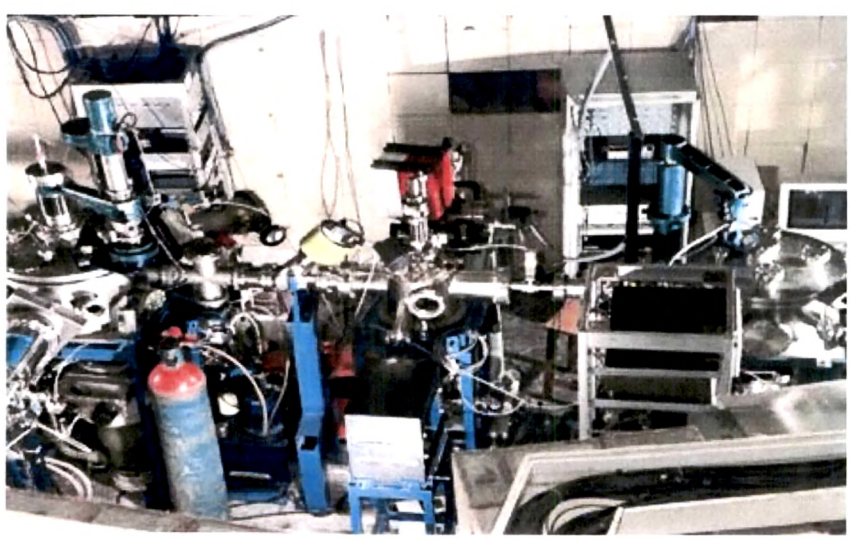

Fig.2.2 Materials Science Chamber for Irradiation

Irradiation procedure

The irradiation process for materials generally carried out at the materials science beam line facility of IUAC New Delhi. This beam line is at 15° angle with respect to the direction of the unswitched direct beam. The beam line is maintained at ultra-low pressure of the order of 10^{-9} Torr and the irradiation is carried out in high vacuum target chamber (HVC). It is fixed in Material Science beam line of Pelletron (Fig 2.2). It has arrangement of temperature control from low temperature to high temperature, dose control which includes positive bias to the target for secondary electron suppression (Faraday cup) and proper mechanical support and alignment. The vacuum in the target chamber is generally maintained below 10^{-6} Torr. A large number of samples can be mounted on all the four sides of a specially designed ladder, which is 10 cm long copper block of rectangular cross-section. Each sample was fixed on the ladder with the help of silver paste. Conducting path was provided by using a line of silver paste from the top surface of the sample to the copper block. The target ladder is inserted in the HVC from the top. Keeping beam current constant, irradiation is carried out at room temperature. By using magnetic quadruple and a steerer the beam is focused on the target. For attaining uniform irradiation the beam is scanned in a desired cm^2 area with the help of a magnetic scanner. The ion fluence is estimated using the ladder current and the current integrator.

2.2.2 Calculation of range and energy loss by SRIM code:

Stopping and Range of Ions in Matter (SRIM) is a group of computer programs which calculate interaction of ions with matter; the core of SRIM is a program. SRIM is based on a Monte Carlo simulation method, namely the binary collision approximation with a random selection of the impact parameter of the next colliding ion. As the input parameters, it needs the ion type and energy (in the range 10 eV – 2

GeV) and the material of one or several target layers. SRIM uses several different stopping theories to evaluate the accuracy of experimental stopping powers. Specifically, calculations are made for all ions in individual targets (which eliminates common difficulties with target dependent quantities such as shell corrections and mean ionization potentials.). Calculations are also made of one heavy ion in all solids, which eliminates some of the difficulties with ion dependent quantities such as the degree of ion stripping. Also, calculations are made from fundamental theories like the Brandt–Kitagawa theory and LSS theory [15].

This is very efficient calculation made up by statistical algorithms which allow the ions to jumps between calculated collisions and then averaging the collision over the applied range. During the collisions, the ion and atom have a screened Coulomb collision, including exchange and correlation between the overlapping electron shells. The ion has long range interactions creating electron excitations and plasmons within the target. These are described by including description of target's collective electronic structure and inter atomic bond structure when the calculation is set up. The charge state of ion within the target is described using the concept of effective charge which depends on velocity of ion and cloud of electrons in the long range screening. The particle losses its energy after each collision by the so called nuclear energy loss which transfer the momentum to the target during collision. Like this it is stopped at or on the surface of the target material.

The SRIM code can be used to compute the ion distribution, detailed calculation for damage cascades, calculation of surface sputtering, electron/neutron/photon cascades, various ion angle/energy/positions, stopping power for ions in gases and compounds.

In the present work, we have estimated the projected range, nuclear stopping power and electronic stopping power of 85 MeV C ions and 120 MeV Si ions in PMMA and PS using SRIM-2003[16].

Results obtained by SRIM-2003 code:

When energetic charged ion strikes on polymeric materials, it loses its energy by two mechanisms known as electronic stopping and nuclear stopping. The projected range, electronic stopping power, nuclear stopping power for 85 MeV C beam and 120 MeV Si beam in PMMA and PS composites was mentioned in Table 2.2.

Table 2.2 Projected ranges for Polymer composites

Sample name	C-ion		
	Projected range μm	Electronic loss eV/Å	Nuclear loss eV/Å
PMMA film	105	4.90×10^{1}	2.79×10^{-2}
PMMA+Ag	112	4.90×10^{1}	2.79×10^{-2}
PMMA+Ni	99.31	5.60×10^{1}	3.10×10^{-2}
PMMA+Cu	105	5.16×10^{1}	2.89×10^{-2}
PS film	104	5.32×10^{1}	2.89×10^{-2}
PS+Ag	109	5.31×10^{1}	2.89×10^{-2}
PS+Ni	98.12	5.98×10^{1}	3.19×10^{-2}
PS+Cu	99	5.38×10^{1}	2.90×10^{-2}

Sample name	Si-ion		
	Projected range	Electronic loss	Nuclear loss
PMMA film	32	2.81×10^{2}	2.65×10^{-1}
PMMA+Ag	36.8	2.81×10^{2}	2.65×10^{-1}
PMMA+Ni	31.72	3.19×10^{2}	2.49×10^{-1}
PMMA+Cu	33.75	3.01×10^{2}	2.32×10^{-1}
PS film	33	3.04×10^{2}	2.33×10^{-1}
PS+Ag	35	3.08×10^{2}	2.93×10^{-1}
PS+Ni	32	3.18×10^{2}	2.43×10^{-1}
PS+Cu	34	3.10×10^{2}	2.33×10^{-1}

In all the cases, maximum energy of the ion beam was lost by electronic interactions. The thickness of polymer sample is larger than the projected range of the beam in the polymer. Hence the beam was stopped in the polymer and maximum dissipation of heat took place at the end. The composites show a lower projected range due to increase in density after doping of filler. This implies that the most of energy loss was due to the electronic energy loss.

2.2.3 Irradiations:

The composite films of different concentrations of metal nanoparticles powder in PMMA and PS were prepared by casting method in which THF and toluene is used as a solvent respectively. These films were irradiated with 85 MeV C- ions and 120 MeV Si-ions at fluence of 1×10^{11}, 1×10^{12} ions/cm^2 at IUAC, New Delhi, India. The ion beam was defocused using a scanning system, so that an area of 1.0 x 1.0 cm^2 was uniformly irradiated. The beam current was kept low (0.5 pnA) to suppress thermal

decomposition and was monitored intermittently with a Faraday cup. The details of irradiation upon samples are shown below in Table2.3.

Table 2.3 Irradiation details of the samples

Sr No	Sample	Fluence (ions/cm^2)	Energy and ions
1.	Pure PMMA	1 x10^{11}, 1 x 10^{12}	85 MeV Carbon, 120 MeV Silicon
	PMMA+5% Ag	1 x10^{11}, 1 x 10^{12}	85 MeV Carbon, 120 MeV Silicon
	PMMA+10% Ag	1 x10^{11}, 1 x 10^{12}	85 MeV Carbon, 120 MeV Silicon
	PMMA+15% Ag	1 x10^{11}, 1 x 10^{12}	85 MeV Carbon, 120 MeV Silicon
2.	PMMA+5% Ni	1 x10^{11}, 1 x 10^{12}	85 MeV Carbon, 120 MeV Silicon
	PMMA+10% Ni	1 x10^{11}, 1 x 10^{12}	85 MeV Carbon, 120 MeV Silicon
	PMMA+15% Ni	1 x10^{11}, 1 x 10^{12}	85 MeV Carbon, 120 MeV Silicon
3.	PMMA+5% Cu	1 x10^{11}, 1 x 10^{12}	85 MeV Carbon, 120 MeV Silicon
	PMMA+10% Cu	1 x10^{11}, 1 x 10^{12}	85 MeV Carbon, 120 MeV Silicon
	PMMA+15% Cu	1 x10^{11}, 1 x 10^{12}	85 MeV Carbon, 120 MeV Silicon
4.	Pure PS	1 x10^{11}, 1 x 10^{12}	85 MeV Carbon, 120 MeV Silicon
	PS+ 5% Ag	1 x10^{11}, 1 x 10^{12}	85 MeV Carbon, 120 MeV Silicon
	PS+ 10% Ag	1 x10^{11}, 1 x 10^{12}	85 MeV Carbon, 120 MeV Silicon
	PS+ 15% Ag	1 x10^{11}, 1 x 10^{12}	85 MeV Carbon, 120 MeV Silicon
5.	PS+ 5% Ni	1 x10^{11}, 1 x 10^{12}	85 MeV Carbon, 120 MeV Silicon
	PS+ 10%Ni	1 x10^{11}, 1 x 10^{12}	85 MeV Carbon, 120 MeV Silicon
	PS+ 15% Ni	1 x10^{11}, 1 x 10^{12}	85 MeV Carbon, 120 MeV Silicon
6.	PS+ 5% Cu	1 x10^{11}, 1 x 10^{12}	85 MeV Carbon, 120 MeV Silicon

	PS+ 10% Cu	1 x10^{11}, 1 x 10^{12}	85 MeV Carbon, 120 MeV Silicon
	PS+ 15% Cu	1 x10^{11}, 1 x 10^{12}	85 MeV Carbon, 120 MeV Silicon

2.3 Experimental characterization techniques

2.3.1 X-ray Diffraction (XRD):

X-ray diffraction (XRD) is a non-destructive analytical technique for identification and quantitative determination of long-range order in various crystalline compounds and also reveals information regarding chemical composition and physical properties. X-rays are electromagnetic radiation which generated by electrons of high energy strike on heavy metal target. When electrons hit the material, some of the electrons will approach the nucleus of the metal atoms where they are deflected because of their opposite charges. This deflection causes the energy of the electron to decrease, and this decrease in energy which resulting an x-ray.

X-rays interact with electrons in atoms. When x-rays collide with electrons, some x-rays from the incident beam are deflected away from the incident direction. If the wavelengths of these scattered x-rays remain unchanged, the process is called an elastic scattering (Thompson Scattering) in that only momentum is transferred during collision [17]. These are the x-rays that are measured in diffraction experiments. They carry information about the electron distribution in materials. On the other hand, during inelastic collision (Compton Scattering), x-rays transfer some of their energy to the electrons and so the scattered x-rays will have different wavelength than the incident x-rays.

Diffraction phenomenon is the consequence of x-ray radiation being scattered by atoms regularly arranged in a lattice possessing interatomic distances of a magnitude comparable to the wave length of the incident radiation. X-rays diffracted from different atoms interfere with each other. If the atoms are arranged in a periodic fashion, as in the case of crystals, the peaks in the interference pattern will correspond to the distribution of atoms. The peaks in an x-ray diffraction pattern are directly related to the atomic distances by Bragg's law [18].

$$n\lambda = 2d\sin\theta \qquad (2.2.2)$$

where, λ is the wavelength of x-ray, d is the inter-planar distance, θ is the scattering angle and n an integer representing the order of the diffraction peak, as shown in Fig. 2.3.

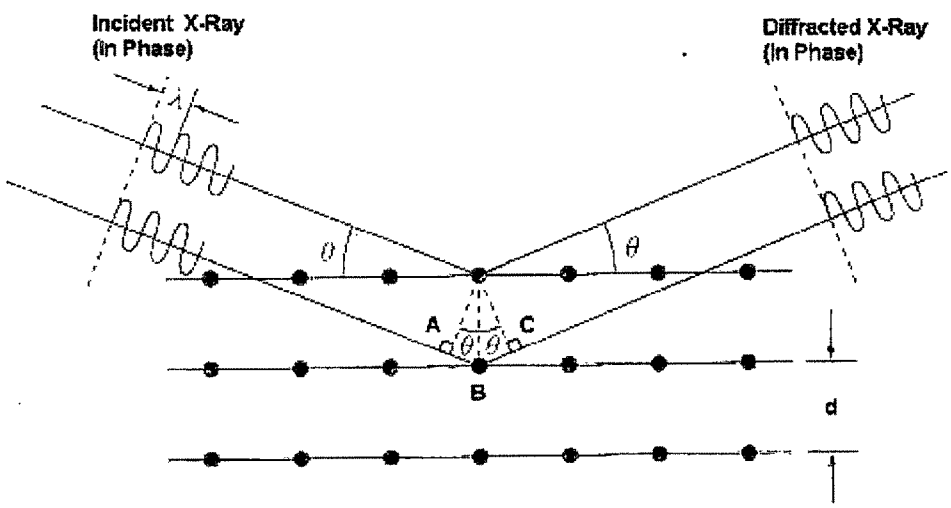

Fig. 2.3 Schematic of Bragg's law

X-ray diffraction data can be collected by using either reflection or transmission geometry as shown in Fig. 2.4(a, b). In the reflection mode, x-rays scattered or reflected from the sample are detected as shown in Fig. 2.4 (a). The reflected x-rays

interfere with each other such that in the diffractogram, intense peaks are obtained at corresponding d values, according to the Bragg's law.

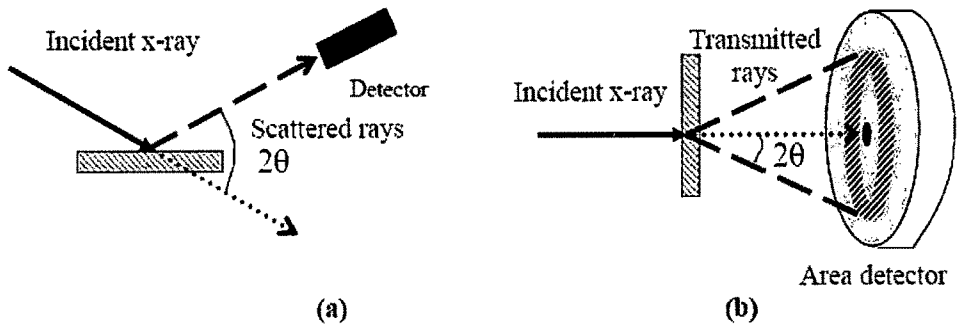

Fig. 2.4 Schematic of x-ray diffraction geometries (a) reflection mode (b) transmission mode

The peak position, intensity, and shape provide important information about the long-range order in the material. For example, the apparent crystal size (L) can be quantitatively calculated by Scherrer's formula [19]

$$b = K\lambda/L\cos\theta \qquad (2.2.3)$$

Where b is FWHM in radians, λ is the wavelength of X-ray beam (1.5418 Å), L is the crystallite size in Å, K is a constant which varies from 0.89 to 1.39, but for most of the cases it is close to 1.

In the transmission mode, an area detector detects the x-rays transmitted through the sample. A circular cone of transmitted rays is incident on the detector, giving a circular ring like pattern as shown in the Fig. 2.4 (b). The radius of the circular ring corresponds to the inter-planar distance. X-Ray Diffraction (XRD) uses the "fingerprint" of a crystalline material to allow identification of unknown phases in a mixture. It is commonly used in the engineering, geological and materials sciences for

applications such as corrosion studies, material fabrication, analysis of combustion products, mineral identification and determination of lattice parameters.

In the present study, the structural studies were carried out by X-ray powder diffractometer (Bruker AXS D8 Advance) with Cu K_α radiation (1.5418 Å) in a wide range of Bragg angles ($10^\circ \leq 2\theta \leq 80^\circ$).

2.3.2 Differential Scanning Calorimetry (DSC):

DSC, is a thermo analytical technique in which the difference in the amount of heat required to increase the temperature of a sample and reference are measured as a function of temperature. Both the sample and reference are maintained at nearly the same temperature throughout the experiment. Generally, the temperature program for a DSC analysis is designed such that the sample holder temperature increases linearly as a function of time. A sample of known mass is heated or cooled and the changes in its heat capacity are tracked as changes in the heat flow. This allows the detection of transitions like melts, glass transitions, phase changes, and curing. Because of this flexibility, DSC is used in many industries including pharmaceuticals, polymers, food, paper, printing, manufacturing, agriculture, semiconductors, and electronics as most materials exhibit some sort of transitions.

A solid material can be amorphous, crystalline, or a combination of the two. Using Differential Scanning Calorimetry (DSC), one can better understand phase transitions and reactions in materials, and how they contribute to the properties and characteristics of the material.

One of the most widely used techniques to measure T_g and T_m is differential scanning-calorimetry (DSC) [20-22]. The signal in a DSC experiment is related to the

difference between the "thermal response" of a small (10 to 30 mg) polymer sample and reference cell (empty) in two separate aluminium pans. The two are heated and cooled at the same rate or maintained at a constant temperature, as illustrated in Fig.2.4. Thermocouple junctions just underneath each position monitor both the temperature of the sample side T_s, and the difference between the temperature of sample side and the temperature of reference, $\Delta T = T_r - T_s$. If the cell is empty and thermally symmetric, the temperature of the reference side will always be the same as the temperature of the sample side irrespective of heating and cooling. The values of specific heat, C_p, may be obtained from the recorded heat-flow rate by calibration with a pure compound such as sapphire for which C_p is known precisely at different temperatures from calorimetry measurements.

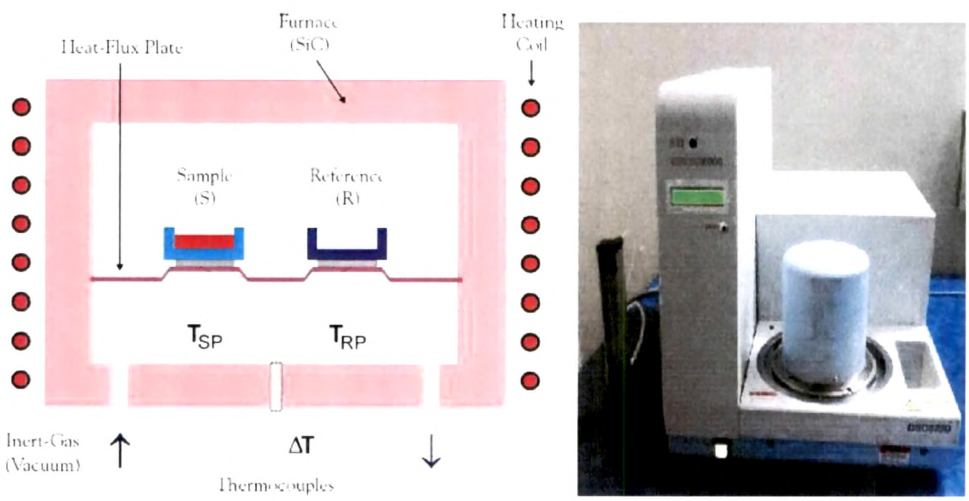

Fig. 2.5 Schematic of DSC

A discontinuity in C_p (i.e., $\Delta C_p = C_p^{\,l} - C_p^{\,g}$), characteristic of a second-order transition, is observed at the polymer T_g that is often identified as the temperature at the midpoint of the step change in C_p (i.e., at $\Delta C_p/2$).

For many amorphous polymers, T_g (K) and ΔC_p (J g^{-1} K^{-1}) are related by the approximate relationship that $\Delta C_p \times T_g$ [21]. During heating of a semicrystalline polymer, additional crystallisation may occur at temperatures between T_g and T_m. At T_m, which may be defined as the extrapolated temperature of the initial slope of the melt endotherm, the crystallites begin to melt over a wide range of temperatures. The breadth of the endotherm is much larger than typically observed for pure low-molecular-weight compounds as a consequence of the lower order of perfection of polymer crystallites. By calibration with a low-molecular-weight standard such as benzoic acid, the heat of fusion (ΔQ) of a semicrystalline polymer can be determined from measurement of the area under the melt endotherm recorded by DSC.

The thermal analysis was performed with differential scanning calorimetry (S II EXSTAR 6000, DSC 6220) with the heating rate of 5°C min^{-1} in the present study.

2.3.3 UV-visible spectroscopy:

Ultraviolet spectrometry is based on absorption of light in visible or ultraviolet regionby an analyte, and is used for measuring its concentration in a solution. Asenergy in the form of ultraviolet or visible light is absorbed by a molecule containing π-electrons or non-bonding electrons, these electrons are excited to higher anti-bonding molecular orbitals. Therefore this technique is appropriate for transition metal ions, highly conjugated organic compounds and biological macromolecules as analytes. Energy carried by a photon is inversely proportional to its wavelength; therefore, lower the energy gap between the highest occupied molecular orbital and lowest unoccupied molecular orbital, the longer the wavelength of light a molecule can absorb. The energy gaps between ground and excited states depend on the

chemical nature of the molecule of interest and therefore the wavelength of the light is chosen accordingly for absorption by that molecule.

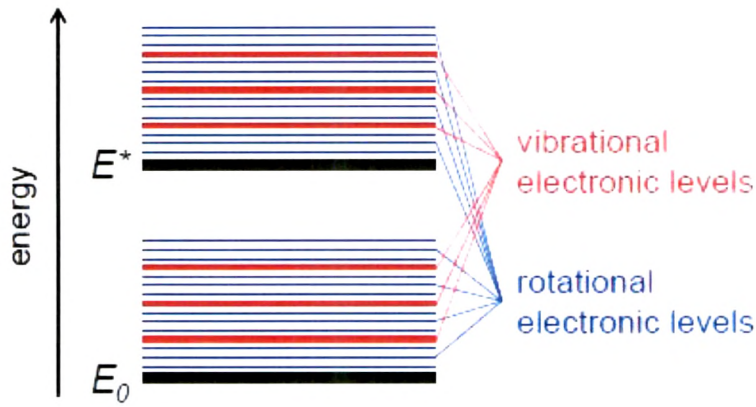

Fig. 2.6 Energy levels diagram

The concentration, c, of the absorbing species and the path length, b, through the solution affect absorbance directly. This relationship can be expressed with Beer's law as $A=\varepsilon bc$, where ε is molar absorptivity, which depends on temperature, pressure and molecular nature of the analyte. Absorbance (A) is the log of ratio of Po is the radiant power of incident beam to the power of transmitted beam P. Po generally corresponds to compensate the attenuation of a beam due to scattering by large molecules, absorption by the solvent or container, and/or reflection.

In ultraviolet or visible radiation absorption, the wavelengths of absorption peaks can be correlated with the types of bonds that exist in the species that is analysed. For this reason, while UV-VIS absorption spectroscopy is used mostly for quantitative determination of compounds containing absorbing groups, molecular absorption spectroscopy is also valuable for identifying functional groups in a molecule. Calibration yielding absorbance vs. concentration relationship is ordinarily made using the absorbance values at a wavelength corresponding to an absorption peak,

because the change in absorbance per unit of concentration is greatest at this point, and thus the maximum sensitivity is realized, where good adherence to Beer's law can be expected.

Instrumentation

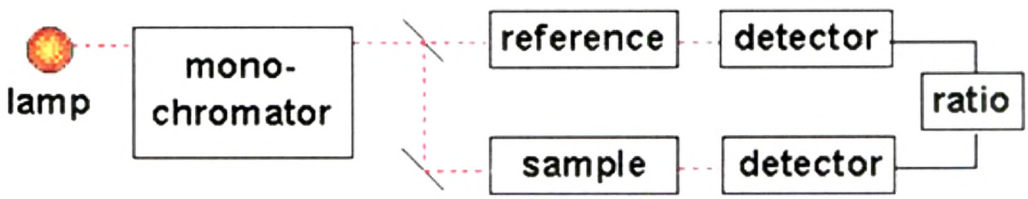

Fig. 2.7 Instrumentation of UV-vis spectrometer

A UV-visible spectrophotometer consists of a light source, a monochromator, sample cell and a detector. Among the light sources, most common are tungsten filament (300-2500nm), deuterium arc lamp (190-400nm) or xenon arc lamp (160-2000nm) or LED for visible wavelengths. Monochromator provides a continuous spectrum using the light coming from the source so that light beam at a specific wavelength can be selected and sent to the solution inside the sample cell. Detector measures the intensities of the light coming from both the blank sample and analyte solution. Hence the absorbance values are calculated for each solution [23-25].

Determinations of band gap

The change in optical properties has been studied by Perkin- Elmer 25 Lambda UV-Visible spectrophotometer in the frequency range 200-800 cm^{-1}. The optical band gap E_g is obtained by Tauc's equation [26]:

$$\omega\varepsilon(\lambda)=(\hbar\omega-E_g)^2 \qquad (2.2.4)$$

where $\varepsilon(\lambda)$ is the optical absorbance and λ is the wavelength. The intersection of the extrapolated spectrum with the abscissa of the plot $\varepsilon^{1/2}/\lambda$ versus $1/\lambda$ yields the gap wavelength λ_g from which the energy gap is derived as $E_g = hc/\lambda_g$.

The number of carbon atoms per cluster (N) can be calculated by following the relation [27]

$$Eg=34.3/\sqrt{N}eV \qquad (2.2.5)$$

where N is the number of carbon atoms per cluster and Eg is the energy band gap.

The number of carbon hexagon rings in the cluster (M) is then found from the relation [27]

$$Eg \approx 2\,|\beta|/\sqrt{M} \qquad (2.2.6)$$

2.3.4 Scanning Electron Microscope (SEM):

A scanning electron microscope (SEM) enables the investigation of specimens with a resolution down to the nanometer scale. It is a type of electron microscope that produces images of a sample surface by scanning it with a high energy beam of electrons in a raster scan pattern. The electrons interact with atoms that make up the sample producing various signals that contain information about the sample's surface topography and composition and other properties such as electrical conductivity.

The main signals which are generated by the interaction of the primary electrons (PE) of the electron beam and the specimen's bulk are secondary electrons (SE) and backscattered electrons (BSE) and furthermore X rays. They come from an interaction volume in the specimen which differs in diameter according to different energies of the primary electrons (typically between 200 eV and 30 keV). The SE come from a

small layer on the surface and yield the best resolution, which can be realized with a scanning electron microscope. The well known topographical contrast delivers micrographs which resemble on conventional light optical images. The BSE come from deeper regions of the investigated material thus giving a lower resolution. As a byproduct of the image giving signals X-rays are produced. They result from ionization processes of inner shells of the atom leading to electromagnetic radiation. The characteristic X-rays give information about the chemical composition of the material. The methods energy dispersive X-ray spectroscopy (EDS) and wavelength dispersive X-ray spectroscopy (WDS) enable the detection of chemical elements from Boron to Uranium in a qualitative and even quantitative manner.

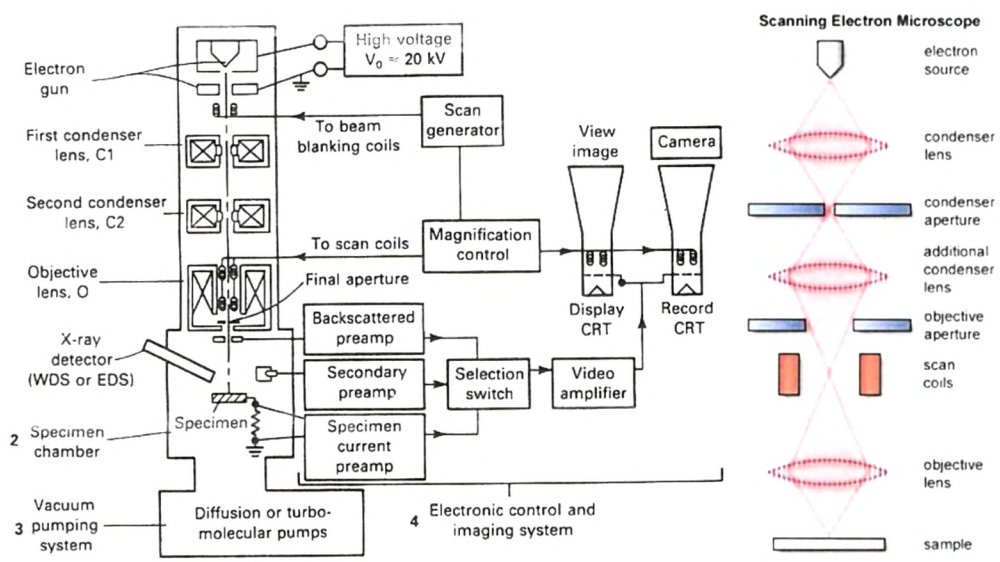

Fig. 2.8 Schematic and working of SEM

Working of SEM:

The schematic of SEM is shown in Fig. 2.8. The Virtual Source at the top represents the electron gun, producing a stream of monochromatic electrons. The stream is condensed by the first condenser lens. This lens is used to both form the beam and

limit the amount of current in the beam. It works in conjunction with the condenser aperture to eliminate the high-angle electrons from the beam. The beam is then constricted by the condenser aperture, eliminating some high-angle electrons. The second condenser lens forms the electrons into a thin, tight, coherent beam and is usually controlled by the "fine probe current knob". A user selectable objective aperture further eliminates high-angle electrons from the beam. A set of coils then "scan" or "sweep" the beam in a grid fashion, dwelling on points for a period of time determined by the scan speed. The final lens, the Objective, focuses the scanning beam onto the part of the specimen desired. When the beam strikes the sample interactions occur inside the sample and are detected with various instruments. Before the beam moves to its next dwell point these instruments count the number of interactions and display a pixel on a CRT whose intensity is determined by this number. This process is repeated until the grid scan is finished and then repeated, the entire pattern can be scanned 30 times per second.

SEM can examine the following information in the samples:

Topography: The surface features of an object or "how it looks", its texture; detectable features limited to a few nanometers.

Morphology: The shape, size and arrangement of the particles making up the object that are lying on the surface of the sample or have been exposed by grinding or chemical etching; detectable features limited to a few nanometers.

Composition: The elements and compounds that the object is composed of and the relative amounts of them.

Crystallographic Information: How the atoms are arranged in the object; direct relation between these arrangements and materials.

2.3.5 Quantum Interference Device (SQUID):

Superconducting Quantum Interference Devices (SQUID) are very sensitive magnetometers capable of measuring extremely small magnetic fields typically of the order of 10^{-17} T [28]. They are based on superconducting loops containing Josephson junctions. Their noise levels in a SQUID are extremely low. A Josephson junction is made up of two superconductors, separated by an insulating layer so thin that electrons can pass through it. A SQUID consists of tiny loops of superconductors employing Josephson junctions to achieve superposition: each electron moves simultaneously in both directions. Because the current is moving in two opposite directions, the electrons have the ability to perform as qubits (that theoretically could be used to enable quantum computing). SQUIDs have been used for a variety of testing purposes that demand extreme sensitivity, including engineering, medical, and geological equipment. Because they measure changes in a magnetic field with such sensitivity, they do not have to come in contact with a system that they are testing.

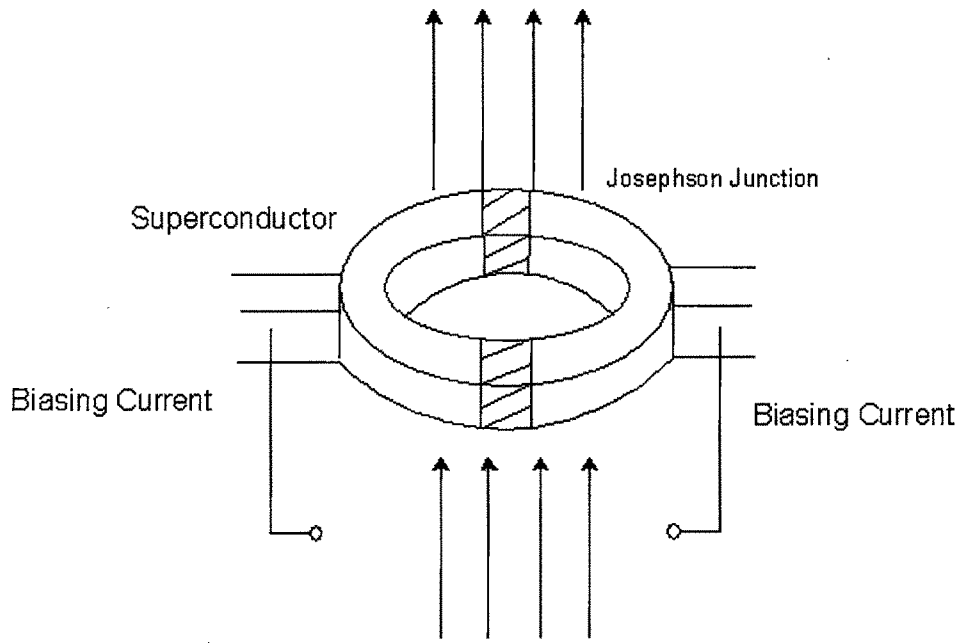

Fig. 2.9 Basic of SQUID

Design of SQUID

SQUID consists of two Josephson junctions connected in parallel. When the SQUID is biased with a current greater than the critical current, the voltage across the SQUID is modulated with the flux treading the SQUID at a period of one flux quantum,

$\Phi_0 \equiv h/2e$ (2.2.7)

Therefore, the SQUID is a flux-to-voltage transducer. This special flux-to-voltage characteristic has enabled researchers to use the device to detect small magnetic field, current, voltage, inductance and magnetic susceptibility. SQUIDs are the most sensi tive devices in detecting the magnetic flux. Low-To SQUID has been used in a wide range of applications, including biomagnetism, susceptometers, nondestructive evaluation, geophysic s scanning SQUID microscope, and nuclear magnetic resonance [28].

2.3.6 Dielectric properties (Impedance phase-gain analyzer):

The evaluation of dielectric parameters namely dielectric permittivity and dielectric loss provide insight into the polarization process that takes place in materials.

Dielectric behavior of a material is arising from the dielectric polarization when the material is under the influence of an external electric field. When an electric field is applied across the sample, there is a shift of charges and electric dipoles are formed inside the material. This shift of charges inside the material causes a net charge to accumulate on the electrodes introducing a capacitance in the system.

When the applied electric field is removed the net dielectric dipole moment formed in the material is supposed to vanish immediately. But this will not happen in reality. Depending on the material there is a delay in coming back to the zero dipole moment state. This delay is due to the various frictional or dissipative forces present in the material. These damping forces cause a power loss and this is termed as the dielectric loss. When a sinusoidally changing electric field is applied across the sample the resulting polarization in the material is lagged by a fixed phase angle due to the dielectric loss. This gives rise to two components of polarization inside the material, these two components can be considered the real and imaginary components of the polarization when represented in a complex plane. Accordingly there are two components for the dielectric permittivity of the material when a sinusoidally varying electric field is applied [29].

Fig. 2.10 shows the Impedance gain phase analyzer/ LCR meter, available at M. S. University of Baroda, Vadodara. This Impedance gain phase analyzer (Solartron-1260) uses powerful microprocessor-controlled digital and analogue techniques to provide a comprehensive range of impedance and frequency response measuring facility. It can be operated for the frequency range from 100 Hz to 10 MHz. Dielectric loss, capacitance and resistance were obtained directly from LCR meter. Using these values conductivity also was calculated.

Fig. 2.10 Impedance phase gain analyzer (Solartron 1260)

(a) AC electrical conductivity:

Electrical conductivity is ability of a material to conduct electric current. An electrical potential difference is applied in a material and its movable charges tend to flow and cause a raise in the electric current. The electrical conductivity is defined as the inverse of the resistivity. In the case of polymers, free electrons which are not attached to the macromolecular chain of polymers, contribute to the conductivity of polymer. Therefore the conductivity of thermoplastic polymers like PMMA, PS, PVC etc are found to be less. There are many methods to improve the conductivity of polymers. In the present study we have reported two effective techniques to get better improvement in conductivity by several orders (a) by doping of metal nanoparticles: which depends upon filler size, shape, orientations and amount of the filler (b) by ion beam irradiation: which depends upon ion species, fluence and energy of ion.

To determine the conductivity the composite materials inserted between the electrodes as shown in figure 2.10.

The a.c. conductivity has been formulated as follows,

Electrical conductivity is defined as the quantity of electrical charge that is transferred per unit of time over a unit of cross sectional area under a unit potential difference gradient;

$$\sigma = \frac{\left(\frac{dq}{dt}\right)}{A\left(\frac{dV}{dx}\right)} \tag{2.2.8}$$

Ohms law describes an equivalent definition as the ratio of the current density to electric field;

$$\sigma = \frac{J}{E} \tag{2.2.9}$$

Where, J is the current density, E is the electric field strength vector which is E=D/ε; where D is the displacement vector of the dipole charges and ε is the complex permittivity of the material. For the parallel plate capacitors, the electric field intensity is the ratio of the potential difference between the plates to the interplate distance (t) so

$$E=V/t \tag{2.2.10}$$

Since Q/A=Vε/t and J =dq/dt, Q/A=q

$$\text{So } J= d/dT(V\varepsilon/t) = (\varepsilon/ t) (dV/dT) = (\varepsilon/ d)Vj\ \omega \tag{2.2.11}$$

Substituting for E and J in equation

$$\sigma_{a.c.} = J/E = \varepsilon j\omega =(\varepsilon- j\varepsilon'')j\omega= \varepsilon j\omega + \varepsilon''\omega \tag{2.2.12}$$

For the a.c. conductivity to be a real so must neglect j

$$\sigma_{a.c.} = \omega\varepsilon'' \tag{2.2.13}$$

When the applied electric field is removed the net dielectric dipole moment formed in the material is supposed to vanish immediately. But this will not happen in reality.

Depending on the material there is a delay in coming back to the zero dipole moment state. This delay is due to the various frictional or dissipative forces present in the material. These damping forces cause a power loss and this is termed as the dielectric loss. When a sinusoidally changing electric field is applied across the sample the resulting polarization in the material is lagged by a fixed phase angle due to the dielectric loss. This gives rise to two components of polarization inside the material, one is in phase and the other is 90° out of phase. These two components can be considered the real and imaginary components of the polarization when represented in a complex plane. Accordingly there are two components for the dielectric permittivity of the material when a sinusoidally varying electric field is applied.

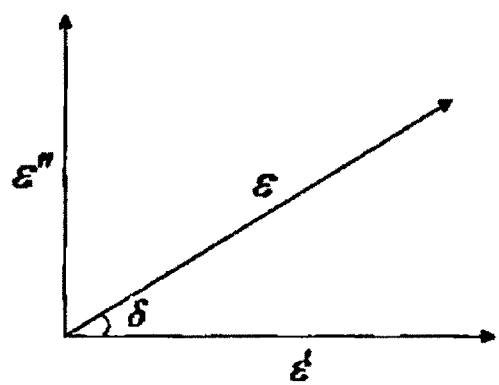

Fig. 2.11 Representation of complex permittivity

$\varepsilon' = \varepsilon \cos\delta$ (2.2.14)

$\varepsilon'' = \varepsilon \sin\delta$ (2.2.15)

$\tan\delta = \varepsilon''/\varepsilon'$ (2.2.16)

substituting the value in (2.2.13) and we get

$\sigma_{ac} = \omega\varepsilon \tan\delta$ (2.2.17)

Where, $\omega = 2\pi f$ and $\varepsilon = \varepsilon_0\varepsilon_r$ (ε_r is the relative permittivity and ε_0 is permittivity of free space).

$\sigma_{ac} = 2\pi f \tan\delta\ \varepsilon_0\varepsilon_r$ (2.2.18)

The dielectric constant can be calculated by

$\varepsilon_r = C_p \times t / \varepsilon_0 A$ (2.2.19)

From the relation (2.2.18) and (2.2.19) we can get the final expression

$\sigma_{ac} = 2\pi f \tan\delta\, C_p\, t/A = 2\pi f D\, C_p\, t/A$ (2.2.20)

To calculate the ac conductivity of polymer we have used this relation.

Where, D = tanδ which is directly measured from LCR meter, C_p is the capacitance of the material, A and t are the area of electrode and thickness of sample respectively.

(b) Dielectric constant:

In the electronic and electrical industry, capacitor represents one of the most fundamental devices. It serves the purpose of filtering unwanted signals, of allowing alternating current (AC) signals to pass while blocking direct current (DC). It can act as a battery or as a power source. In general the capacitor is a very versatile device, and as such, it has many properties based on the application where it is used.

The defining characteristic of a capacitor is its ability to store electric charge. This ability is called its capacitance C, and is defined by the following relationship:

$C=Q/V$ (2.2.21)

Where, Q is the stored charge and V is the potential difference connected across the electrodes. The SI unit of capacitance is the farad, which is 1 coulomb per volt. The capacitance of a capacitor with flat, parallel electrodes separated by vacuum is directly proportional to the active electrode area A and inversely proportional to the separation d as described by the following equation:

$C=\varepsilon_0 A/t$ (2.2.22)

where ε_0 is a universal constant having the value of 8.85×10^{-12} F/m.

When two parallel electrodes are separated by a distance t with dielectric materials, the capacitance can be expressed as:

$C=\mathcal{E}_0\mathcal{E}rA/t$ (2.2.23)

where $\mathcal{E}r$ is the relative permittivity.

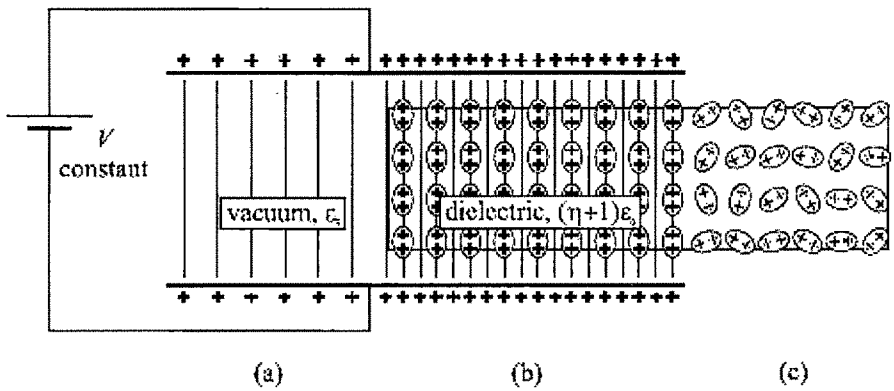

Fig. 2.12 Polarization in Dielectric (a) vacuum capacitor, (b) polarised dipoles in the dielectric inserted between the capacitor plates, (c) random dipoles when no electric field is applied.

From the equation (2.2.23) we can see how effective a capacitor to store energy depends on the material used for the dielectric. And each material has unique dielectric permittivity and dielectric strength, which is the maximum voltage that can be applied across the electrodes without breakdown. If breakdown occurs, current will flow between the electrodes.

(c) Dielectric Loss:

The dielectric loss is a measure of energy loss in the dielectric during AC operation, which is a material property and does not depend on the geometry of capacitor. Usually the dielectric loss, expressed as the loss tangent (tan δ) or dissipation factor (Df) can be defined as

$\tan \delta = \mathcal{E}''/\mathcal{E}'$ (2.2.16)

In general, dielectric loss of the dielectric material is resulted from distortional, dipolar, interfacial, and conduction loss. The distortional loss is related with electronic and ionic polarization mechanisms. The interfacial loss originates from the excessive

polarized interface induced by the fillers and specifically the movement or rotation of the atoms or molecules in an alternating electric field. The conduction loss is attributed to the dc electrical conductivity of the materials, representing the flow of actual charge through the dielectric materials [30, 31].

References:

[1] Brydson, Plastics Materials, Butterworths (1989).

[2] Campo, E. Alfredo, the Complete Part Design Handbook, Hanser (2006).

[3] Osswald, et al, International Plastics Handbook, Hanser (2006).

[4] Strong, Plastics Materials and Processing, Prentice Hall (2000).

[5] Rajesh Kumar Srivastava, T. N. Narayanan, A. P. Reena Mary, M. R. Anantharaman, Anchal Srivastava, Robert Vajtai, Pulickel M. Ajayan, Appl. Phys. Lett., 99 (2011) 113116.

[6] L.C. Costa, F. Henry, M.A. Valente, S.K. Mendiratta, A.S. Sombra, European Polymer Journal 38 (2002) 1495–1499.

[7] Pranay Jain, Vibor Aggarwal, International Journal of Nano and Material Sciences, 1(2) (2012) 108-120.

[8] R. C. Doty, T. R. Tshikhudo, M. Brust, D. G. Ferning, Chem. Mater. 17 (2005) 4630.

[9] P S Guo, Z Sun, Y W Chen, Z H Zheng, Mater. Lett. 60 (2006) 966.

[10] Zh S Luo, Ch L Chen, D J Zhao, Sh L Luo and Zh Ch Li, Chem. Phys. Lett. 421 (2006) 584.

[11] Huazhi Wang, Xinli Kou, Jie Zhang, Jiangong Li, Bull. Mater. Sci., Vol. 31 (2008) 97.

[12] Xiao-Min Ni, Xiao-Bo Su, Zhi-Ping Yang, Hua-Gui Zheng, Journal of Crystal Growth 252 (2003) 612.

[13] M.S. Yeh, Y.S. Yang, Y.P. Lee, H.F. Lee, Y.H. Yeh, C.S.Yeh, J. Phys. Chem. B R., 103 (1999) 6851.

[14] George H. Chan, Jing Zhao, Erin M. Hicks, George C. Schatz, Richard P. Van Duyne, Nano letters, 7 (2007) 1947.

[15] J. Lindhard, M. Scharff, H.E. Schiott, Kgl. Danske Vid. Sels. Mat.-Fys. Medd. 33 (1963) 1.

[16] J. F. Ziegler, code SRIM 2006, The stopping range of ions in matter (IBM research), New York, USA (2006).

[17] H. P. Klugg, L. E. Alexander, X-ray diffraction procedures; John Wiley & Sons: USA (1974).

[18] W.L. Bragg, "The Diffraction of Short Electromagnetic Waves by a Crystal". *Proceedings of the Cambridge Philosophical Society* 17: 43–57(1913).

[19] P. Scherrer, Gott. Nachar, 2 (1918) 98–100.

[20] P. J. Haines, "Thermal Methods of Analysis", Blackie Academic and Professional, 1995, p.63. ,

[21] J. R. Fried, "Polymer Science and Technology", Prentice Hall PTR, 1995, p.153.

[22] M. P. Stevens, "Polymer Chemistry", Oxford University Press, 1999, p.149.

[23] Skoog, A.D., Leary J. J., "Principles of Instrumental Analysis", 4th ed., pp. 123-173.

[24] Ewing, W.Galen, "Instrumental Methods of Chemical Analysis", 4th ed., pp. 34-42, 63-74.

[25] Willar, Merritt, Dean, Settle, "Instrumental Methods of Analysis", 6th ed., pp.66-78.

[26] A. K. Srivastava, H. S. Virk, J. Polym. Mater. 17 (2000) 325-328.

[27] A. Das, S. Dhara and A. Patnaik, Physical Rev B 59 (1999) 11069

[28] Hong-Chang Yang et al, Tamkang Journal of Science and Engineering, 6, No. 1, (2003) 9-18.

[29] B. Tareev, Physics of Dielectrics Materials, MlR Publishers (1975), Moscow

[30] J. Lu, K. S. Moon and C. P. Wong, Proceedings of 11th International Symposium on Advanced Packaging Materials, pp. 88-92 (2006).

[31] J. Lu, K. S. Moon, J. Xu and C. P. Wong, 231st American Chemical Society Meeting, Atlanta, GA, March 26-30 (2006).